Supplementary Information

Cohesive self-organization of mobile microrobotic swarms

Berk Yigit[#], Yunus Alapan[#], and Metin Sitti[*]

Physical Intelligence Department, Max Planck Institute for Intelligent Systems, 70569 Stuttgart, Germany

[*] E-mail: sitti@is.mpg.de

[#] The authors contributed equally and share the first authorship.

Supplementary Note 1: Applied magnetic fields

Precessing magnetic field is defined by two angles. Precession angle Ψ is the angle between the axis of precession (***w***) and the magnetic field vector (***B***), and the tilt angle ϑ is the angle between the precession axis and the normal vector to the planar substrate surface (*i.e.*, z-axis) (Fig. 1a). Applied magnetic field is varied in time by revolving the magnetic field vector about the precession axis, with angular velocity Ω via the following mathematical operation:

$$B(t) = B_0\left(I + \sin(\Omega t)[w]_\times + (1 - \cos(\Omega t))[w]_\times^2\right)n_0 \qquad \text{(Eq. S1)}$$

where $B_0 = \|B\|$ is the magnetic field magnitude, t is time, $\boldsymbol{I}$ is the identity matrix, $[\,]_\times$ is the cross-product operator, $\boldsymbol{w} = (0, \sin(\vartheta), \cos(\vartheta))$, and $\boldsymbol{n}_0 = (0, \sin(\vartheta + \Psi), \cos(\vartheta + \Psi))$ is the magnetic field vector at $t = 0$.

Supplementary Note 2: Magnetic interactions between chains

For calculation of magnetic interaction forces between two chains (Figs. 2a-b and S2), we considered that each chain consists of n paramagnetic particles and precess by following the

magnetic field given by Eq. S1. Distance vector pointing from the j^{th} particle to i^{th} particle is denoted by $\boldsymbol{R}_{ij} = \boldsymbol{R}_j - \boldsymbol{R}_i$, where $\boldsymbol{R}_i$ and $\boldsymbol{R}_j$ denote their respective position vectors. The induced magnetic dipole moment $\boldsymbol{m}_i$ of each particle is given by $m_i = v_p \chi B/\mu_0$, where v_p is the particle volume, χ is the volumetric magnetic susceptibility and μ_0 is the vacuum permeability. The interaction force between two magnetic dipoles is calculated with the following equation[1],

$$f_{m,ij} = \frac{3\mu_0}{4\pi R^4}\left(\frac{R_{ij}(m_i.m_j) + m_i(R_{ij}.m_j) + m_j(R_{ij}.m_i)}{R} - \frac{5R_{ij}(m_i.R_{ij})(m_j.R_{ij})}{R^3}\right)$$

(Eq. S2)

Following, the time-averaged magnetic force acting between two chains can be calculated by summing the interaction forces between particles and averaging over a precession cycle,

$$F_m = \Omega \int_0^{1/\Omega} \sum_{i \neq j} f_{m,ij}(t)dt \qquad \text{(Eq. S3)}$$

where the summation is performed over each particle pair i, j belonging to chains. Observing Eqs. S2 and S3, the strength of the magnetic force between two chains varies with the following proportionality:

$$F_m \propto n^2\left(\frac{4\pi\,(a^3\chi B)^2}{3\mu_0 \quad r^4}\right) \qquad \text{(Eq. S4)}$$

where r is the distance between two chains. Therefore, for a pair of chains separated by a distance of one chain length ($r = 2na$), a characteristic magnetic interaction force can be defined as:

$$F_0 = \left(\frac{\pi}{12\mu_0} \frac{(a\chi B)^2}{n^2} \right)$$ (Eq. S5)

Supplementary Note 3: Numerical model for simulating flow fields around a single chain

Flow field generated by the precession of a chain near a wall was calculated with simulations using Stokes flow singularities. Flow velocity at a given position in space $\boldsymbol{v}_h(\boldsymbol{r})$ due to a collection of particles on which a force $\boldsymbol{f}_j(\boldsymbol{R}_j)$ (*i.e.*, a Stokeslet) acts can be obtained with the following equation,

$$v_h(r) = \sum_j J(r,R_j).f_j(R_j)$$ (Eq. S6)

In an unbounded fluid, $J(r,R_j)$ is given by the Oseen tensor,

$$J(r,R_j) = \frac{1}{8\pi\mu}\left(\frac{I}{|r-R_j|} + \frac{(r-R_j)\otimes(r-R_j)}{|r-R_j|^3} \right)$$ (Eq. S7)

Where μ is the dynamic viscosity of the fluid. Wall effects can be accounted for by modifying Eq. S7 through the image system of hydrodynamic singularities satisfying no-slip boundary conditions at the surface, which was formulated in the work of Blake and Chwang[2] and was also used in our simulations. The image system of a Stokeslet at $\boldsymbol{R}_i = (x, y, h)$ near an infinite planar no-slip wall consists of an opposite signed Stokeslet, and an additional Stokes-doublet and a source doublet positioned at $\boldsymbol{R}_{im,i} = (x, y, -h)$, where h indicates the distance from the wall (at $z = 0$)[2]. Flow velocities presented in Figs. 2c-d and Fig. S3 were obtained by calculating time-varying flow field generated by a chain and taking its average over a precession cycle.

Supplementary Note 4: Numerical model for simulating the chain dynamics

For simulating the dynamics of motile self-assembled chains (Figs. 2e-h and S4, Video S2), we model the dynamics of the collection of particles that constitute the chains, whose equation of motion is given by,

$$\dot{R}_i = M_{ij}.(f_{m,j} + f_{b,j} + f_{w,j} + f_{g,j}) \quad \text{(Eq. S8)}$$

where interactions between particles *i* and *j* arise from magnetic dipole-dipole forces ($\boldsymbol{f}_m$), particle-particle ($\boldsymbol{f}_b$) and particle-wall ($\boldsymbol{f}_w$) excluded volume forces, and gravitational ($\boldsymbol{f}_g$) forces. Magnetic dipolar interactions between particles are calculated via Eq. S2. The grand mobility tensor M couples the velocities of particles ($\dot{R}_i$) to the forces acting on each particle through contributions of self and pair hydrodynamic mobility tensors that account for no-slip boundary conditions at the substrate surface[3]. Simulations implement the mathematical expressions for the grand mobility tensor that were provided by Swan and Brady[3]. Following the approach presented by Sing *et al.*[4], particle-particle and particle-wall excluded volume forces were modeled with modified Lennard-Jones force terms,

$$f_b = \frac{\epsilon}{r-2a}\left(\left(\frac{\sigma}{r-2a}\right)^{12} - \left(\frac{\sigma}{r-2a}\right)^{6}\right) \quad \text{(Eq. S9)}$$

$$f_w = \frac{\epsilon}{h-a}\left(\left(\frac{\sigma}{h-a}\right)^{12} - \left(\frac{\sigma}{h-a}\right)^{6}\right) \quad \text{(Eq. S10)}$$

with $\sigma = 0.1a$, h is the distance of a particle from the wall, and ϵ is sufficiently small to neglect attractive terms. $f_g = -\Delta\rho v_p g$ where $\Delta\rho$ is the buoyant density of particles, and g is the gravitational acceleration. Eq. S8 was integrated with an explicit Euler scheme to obtain the trajectories of each particle in chains. Each cycle of chain rotation was divided into 5×10^5 time steps, and simulations were performed for 270 cycles (~30 seconds of real time experiments).

Table S1. Simulation parameters

A	2.5 μm	χ	0.5
B_0	10 mT	$\Delta\rho$	0.05 g/cm^3
$\Omega/2\pi$	3 Hz	μ	0.894 mPa.s

Supplementary Note 5: Reduced-order discrete chain model

For simulating the dynamics of clusters consisting of many chains, calculating the motion of each particle separately is computationally intensive. For this reason, we developed a reduced order simulation that models the dynamic of the collection of chains that constitute the cluster, in which each chain is treated as a discrete point (Fig. S6 and Video S7). This model accounts for the time-averaged magnetic interactions and near-wall hydrodynamic self-propulsion and interactions between chains. The equation of motion for each chain is given by

$$\dot{r}_i = v_{0,i} + \sum_{j \neq i} v_{h,ij} + \sum_{j \neq i} v_{m,ij} \qquad \text{(Eq. S11)}$$

where the velocity of i^{th} chain ($\dot{r}_i$), is the sum of its self-propulsion velocity, $\mathbf{v}_{0,i}$, the velocity of the hydrodynamic flow generated by all its j^{th} neighbours at the position of i^{th} chain, $\mathbf{v}_{h,ij}$, and the displacement velocity due to the magnetic forces imposed by its neighbors, $\mathbf{v}_{m,ij}$.

Self-propulsion of a chain arises from its self-advection under the hydrodynamic flow generated by its precessing motion. Similarly, a chain is also advected by the flow generated by its neighbors. The essential features of hydrodynamic flows were captured by modeling each chain as a rotlet singularity above a solid wall. Specifically, a rotlet solution provides the hydrodynamic velocity field generated by a point torque at Stokes regime. We consider that each chain has an

effective hydrodynamic radius a_h, and its rotation is given with the angular velocity vector Ω. The axis of rotation is tilted from the *z*-axis (*i.e.*, normal to the plane of the substrate) by angle ϑ, therefore, the angular velocity vector can be decomposed into two components which are parallel and perpendicular to the substrate, such that $\boldsymbol{\Omega} = (0, \Omega_{\parallel}, \Omega_{\perp})$ where $\Omega_{\parallel} = \Omega.\sin(\vartheta)$ and $\Omega_{\perp} = \Omega.\cos(\vartheta)$. Chains are located at a distance h from the wall at $\boldsymbol{r} = (x, y, h)$. The solid wall imposes hydrodynamic no-slip boundary conditions, which can be accounted through the image system consisting of a counter-rotating rotlet, and an additional stresslet and a source doublet positioned at $\boldsymbol{r}_{im} = (x, y, -h)$, which was formulated in the work of Blake and Chwang[2]. Thus, the flow velocity at the position of the i^{th} chain is calculated by the following expressions[2,5]:

$$v_{0x,i} = \frac{\Omega_{\parallel,i} a_{h,i}^5}{8h_i^4} \quad \text{(Eq. S12)}$$

$$v_{hx,ij} = \Omega_{\parallel,j} a_{h,j}^3 \left(6h_i \frac{(x_j - x_i)^2}{r_{im,ij}^5} - \frac{h_j - h_i}{r_{ij}^3} + \frac{h_j - h_i}{r_{im,ij}^3} \right) + \Omega_{\perp,j} a_{h,j}^3 \left(\frac{y_j - y_i}{r_{ij}^3} - \frac{y_j - y_i}{r_{im,ij}^3} \right) \quad \text{(Eq. S13)}$$

$$v_{hy,ij} = \Omega_{\parallel,j} a_{h,j}^3 \left(6h_i \frac{(x_j - x_i)(y_j - y_i)}{r_{im,ij}^5} \right) + \Omega_{\perp,j} a_{h,j}^3 \left(\frac{x_i - x_j}{r_{ij}^3} - \frac{x_i - x_j}{r_{im,ij}^3} \right) \quad \text{(Eq. S14)}$$

where $r_{ij} = \left((x_i - x_j)^2 + (y_i - y_j)^2 + (h_i - h_j)^2 \right)^{1/2}$ and $r_{im,ij} = \left((x_i - x_j)^2 + (y_i - y_j)^2 + (h_i + h_j)^2 \right)^{1/2}$.

The first role of $\Omega_{\parallel}$ is self-propulsion, a chain rotating about the *y*-axis would translate in the *x*-direction, which is expressed in Eq. S12. The hydrodynamic velocity field generated by $\Omega_{\parallel}$

in the x - y plane is displayed in Fig. S6a. Flow field has a positive velocity in the x-direction around the rotlet. This leads to an enhancement of translation velocity in the x-direction for neighboring chains as a result of being advected by the flows generated by each other. The $\Omega_\perp$ component of rotation results in a rotating flow in the x - y plane (Fig. S6b), and is the main contributor to the rotation of chains around each other, and leads to the rotation of the cluster.

To calculate $\boldsymbol{v}_{\mathrm{m,ij}}$, we modeled the magnetic interaction force between chains with a time-averaged force that acts along the line connecting chain centers. Magnetic interaction force combines an attractive dipolar term and a repulsive multipolar term, which is given via the following equation:

$$F_{m,ij} = \left[\frac{A}{r^4} + \frac{B}{r^k}\right]\hat{r} \qquad \text{(Eq. S15)}$$

where A and B are the coefficients for dipolar and multipolar contributions, respectively, k is an effective exponent that tunes the stiffness of the multipolar term and $\hat{r}$ is the unit vector pointing from chain i to j. Dipolar interaction has a $1/r^4$ rate of decay, and multipolar interaction has an effective decay rate of $1/r^k$.

For determination of A, we consider the time-averaged effective dipolar interactions between two chains that precess about the z-axis with angle Ψ. The time averaged dipolar coupling strength under precession is given by[6]

$$A = \frac{3\pi}{4\mu_0} m_i m_j \left(\frac{3\cos\Psi - 1}{2}\right) \qquad \text{(Eq. S16)}$$

where the total dipole moment $\boldsymbol{m}_\mathrm{i}$ is given by $\boldsymbol{m}_\mathrm{i} = n\boldsymbol{m}$, where n is the number of particles in the chain and $\boldsymbol{m}$ is the magnetic dipole moment of a single particle. The sign of the term in brackets

depends on the precession angle, which leads to a repulsive interaction ($A > 0$) for $0^\circ \leq \Psi < 54.7^\circ$, and an attractive interaction ($A < 0$) for $54.7^\circ < \Psi \leq 90^\circ$). As discussed in the manuscript, a combination of long-range attraction and a short-range repulsion results in a steady-state distance, r^*, where magnetic interaction force between chains equates to zero, $F_m(r^*) = 0$. Consequently, we obtain $\frac{B}{A} = -r^{*k-4}$, which allows us to re-write Eq. S15 as

$$F_{m,ij} = \frac{A}{r^4}\left[1 + \left(\frac{r^*}{r}\right)^{k-4}\right]\hat{r}. \quad \text{(Eq. S17)}$$

In the simulations, we use the functional form given by Eq. S17, which lets us specify r^* as an input parameter. Eq. S17 tells us that, if A and r^* are known, then the only remaining unknown is k, which tunes the stiffness of the repulsive multipolar interaction. We found that setting k to different values in the range of 6 to 8 produce qualitatively similar results in our simulations. Lastly, $\boldsymbol{v}_{m,ij}$ is calculated by multiplying the magnetic interaction force with the effective mobility of a chain:

$$v_{m,ij} = (6\pi\mu na)^{-1} F_{m,ij}. \quad \text{(Eq. S18)}$$

The reduced-order model successfully captures the essential trends observed in experiments: Chains form cohesive clusters with a characteristic steady-state distance between neighbors, clusters performed rotation and translation, and the cluster velocity increased with number of chains. An example of simulated trajectories is displayed in Fig. S6c and Video S7. In order to achieve a quantitative fit between the model and the experiments for translation and angular velocity of clusters, we need to tune two parameters a_h and h (Figs. S6a-b). An experimental determination of a_h and h is difficult due to the anisotropic shape of chains. Also, a

simplistic estimation by setting them to half chain length ($L/2 = na$) yields predictions far from the experimental observations. For this reason, we performed simulations for different values of h and re-scaled the simulated values via a_h to match the experimental values. Changing h has a small effect on the translational velocity of clusters (Fig. S6a), and shifts the curve for the angular velocity of clusters by a prefactor approximately proportional to $h^{3/2}$ without changing the shape of the curve (Fig. S6b). The curves in Fig. 5c correspond to $h/L = 0.3$ and $a_h/L \sim 0.26$.

Supplementary Note 6: Data analysis

Experimentally, we measure the set of coordinates for the collection of chains i, $\{\boldsymbol{r}_i(t)\}$, where $\boldsymbol{r}_i(t)$ is the position of the center of chain i at different time points t. To find the internal position of chains within the cluster at a desired time point, we need to subtract the mean cluster position and rotation from the set of chain coordinates[7]. Mean cluster position can be obtained by taking the average of chain coordinates, $r_c(t) = (1/N)\sum_i^N r_i(t)$. Therefore, chain positions with respect to the moving cluster center can be obtained by, $\boldsymbol{y}_i(t) = \boldsymbol{r}_i(t) - \boldsymbol{r}_c(t)$. To find the optimal mapping between two sets of chain positions measured at consecutive time points, we are required to find the best rotation matrix $R(t)$ that minimizes the error function, $\sum_i^N [y_i(t+1) - R(t)y_i(t)]^2$, where $t + 1$ denotes the next time point[8]. Finally, internal positions of chains can be obtained after subtracting mean cluster translation and rotation as

$$x_i(t) = R^T(0)\ldots R^T(t-2)R^T(t-1)y_i(t)\,. \qquad \text{(Eq. S19)}$$

Rotational order: Rotational order parameter quantifies the degree of coherence of rotational motion of chains about the cluster center. Rotational order parameter is calculated with the following equation[7],

$$Rotational\ order = \frac{1}{N}\left\| \sum_{i=1}^{N} \frac{y_i(t) \times v_i(t)}{|y_i(t) \times v_i(t)|} \right\| \quad \text{(Eq. S20)}$$

where $v_i = y_i(t+1) - y_i(t)$ is the chain velocity after subtracting the translation velocity of the cluster center. Perfectly coherent rotation results in a rotational order parameter equal to 1, and to 0 for non-coherent motion.

Connectivity: Connectivity is calculated based on the idea that strength of cohesive magnetic interactions that holds the chains together would be proportional to the total attractive magnetic dipolar potential in a cluster with the below formula:

$$Connectivity = \sum_{i \neq j} \frac{n_i n_j}{r_{ij}^3} \quad \text{(Eq. S21)}$$

where r_{ij} is the distance between two chains and $n_{i,j}$ is the number of particles in chains *i*, *j*.

Mean-squared displacement: Mean-squared displacement (MSD) is calculated with the standard formula of

$$MSD(\tau) = \left\langle \left\| x_i(t+\tau) - x_i(t) \right\|^2 \right\rangle \quad \text{(Eq. S22)}$$

where $\langle \cdot \rangle$ is the ensemble average over chains *i*, and time *t*, and τ is the lag time between two time points. "Fluctuation" quantifies the mean-squared positional fluctuation of chains, *i.e.* deviations around their mean positions in the cluster. Fluctuation is calculated with the following formula[9]:

$$Fluctuation = \left\langle \left\| x_i(t) - \bar{x}_i \right\|^2 \right\rangle \quad \text{(Eq. S23)}$$

where $\langle \cdot \rangle$ is the ensemble average over chains i and time t, and $\bar{x}_i$ is the mean position of the i^{th} chain inside the cluster.

References

1. Yung KW, Landecker PB, Villani DD. An Analytic Solution for the Force Between Two Magnetic Dipoles. *Magnetic and Electrical Separation* **9**, 39-52 (1998).
2. Blake JR, Chwang AT. Fundamental singularities of viscous flow. *Journal of Engineering Mathematics* **8**, 23-29 (1974).
3. Swan JW, Brady JF. Simulation of hydrodynamically interacting particles near a no-slip boundary. *Physics of Fluids* **19**, 113306 (2007).
4. Sing CE, Schmid L, Schneider MF, Franke T, Alexander-Katz A. Controlled surface-induced flows from the motion of self-assembled colloidal walkers. *Proceedings of the National Academy of Sciences* **107**, 535-540 (2010).
5. Martinez-Pedrero F, Navarro-Argemí E, Ortiz-Ambriz A, Pagonabarraga I, Tierno P. Emergent hydrodynamic bound states between magnetically powered micropropellers. *Science Advances* **4**, eaap9379 (2018).
6. Tierno P, Schreiber S, Zimmermann W, Fischer TM. Shape Discrimination with Hexapole−Dipole Interactions in Magic Angle Spinning Colloidal Magnetic Resonance. *Journal of the American Chemical Society* **131**, 5366-5367 (2009).
7. Attanasi A*, et al.* Collective Behaviour without Collective Order in Wild Swarms of Midges. *PLOS Computational Biology* **10**, e1003697 (2014).
8. Kabsch W. A solution for the best rotation to relate two sets of vectors. *Acta Crystallographica Section A: Crystal Physics, Diffraction, Theoretical and General Crystallography* **32**, 922-923 (1976).
9. Meinhold L, Smith JC. Fluctuations and Correlations in Crystalline Protein Dynamics: A Simulation Analysis of Staphylococcal Nuclease. *Biophysical Journal* **88**, 2554-2563 (2005).

Supplementary Figures

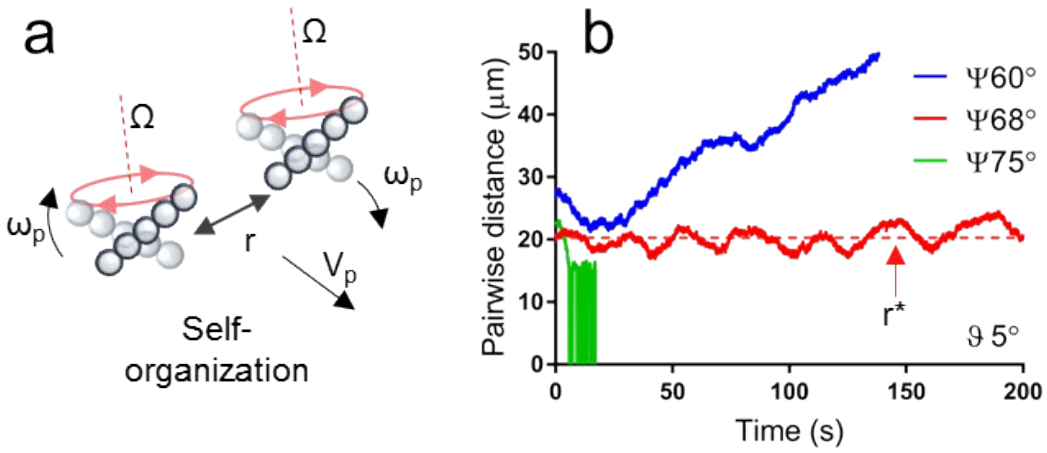

Figure S1. Experimental characterization of pairwise chain interactions (a) Schematic of the two-chain system, r is pairwise distance between chains, V_p is pair velocity and ω_p is pair angular velocity. **(b)** Pairwise distance measurements under diverging ($\Psi = 60^\circ$), cohesion ($\Psi = 68^\circ$) and collapsing ($\Psi = 75^\circ$) states, where r^* denotes the dynamic steady-state distance.

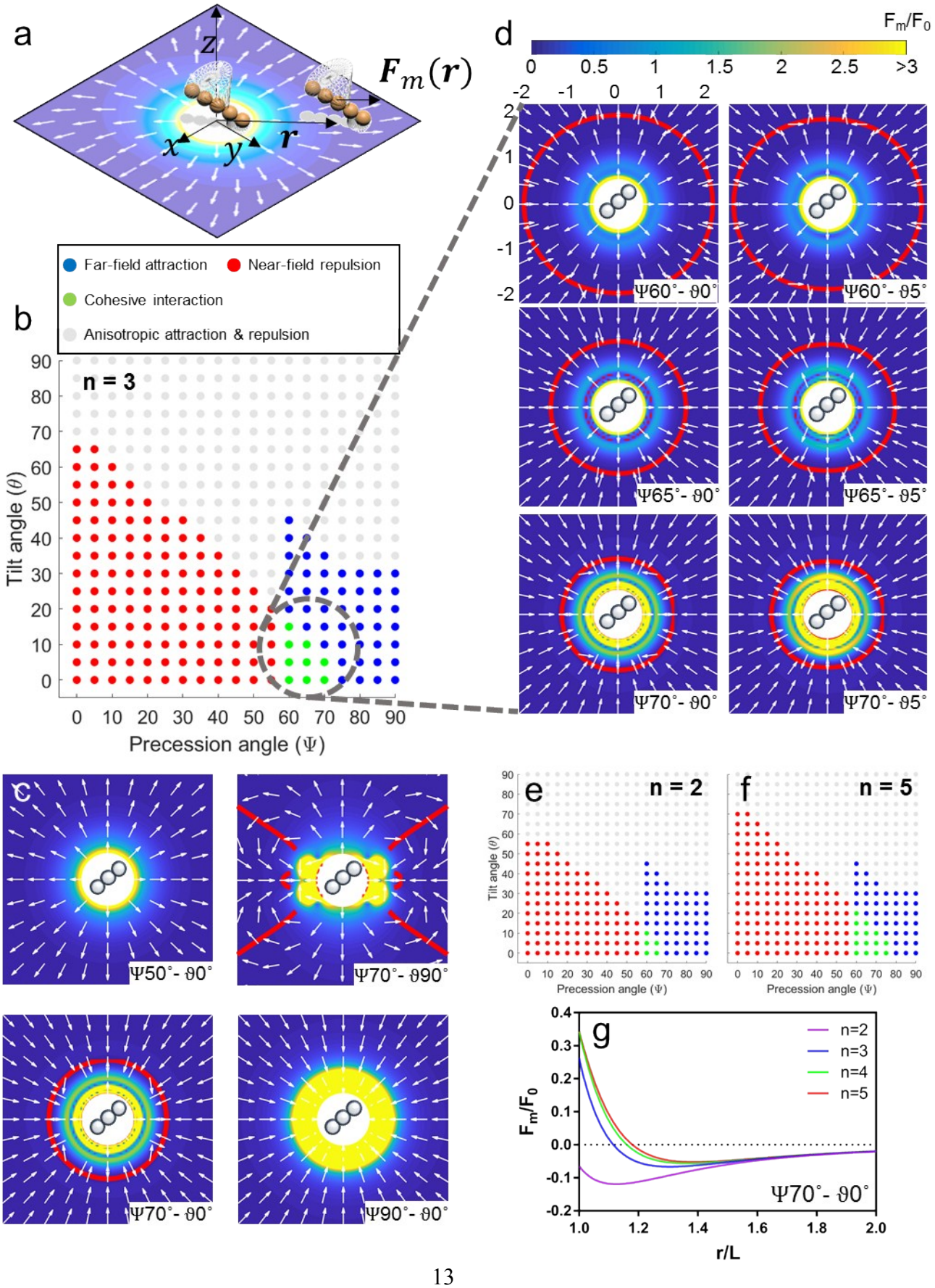
a
z
x
y
r
$F_m(r)$
b
Far-field attraction
Near-field repulsion
Cohesive interaction
Anisotropic attraction & repulsion
n = 3
Tilt angle (θ)
Precession angle (Ψ)
d
F_m/F_0
0
0.5
1
1.5
2
2.5
>3
Ψ60°- ϑ0°
Ψ60°- ϑ5°
Ψ65°- ϑ0°
Ψ65°- ϑ5°
Ψ70°- ϑ0°
Ψ70°- ϑ5°
c
Ψ50°- ϑ0°
Ψ70°- ϑ90°
Ψ70°- ϑ0°
Ψ90°- ϑ0°
e
n = 2
f
n = 5
Tilt angle (θ)
Precession angle (Ψ)
Precession angle (Ψ)
g
n=2
n=3
n=4
n=5
F_m/F_0
Ψ70°- ϑ0°
r/L

Figure S2. Pairwise magnetic interactions between chains. (a) Schematic describes the configuration between two chains used in simulations calculating magnetic interaction forces $\boldsymbol{F}_{\mathrm{m}}$ along the direction of vector $\boldsymbol{r}$ = (x, y, 0) pointing from the first chain at the origin to the second chain. **(b)** Simulated magnetic interaction states between two chains (number of particles per chain, n = 3). States are categorized as follows, far-range attraction ($F_{\mathrm{m}} < 0$ for $r/L = 2$), short-range repulsion ($F_{\mathrm{m}} > 0$ for $r/L = 1$), cohesive interaction ($F_{\mathrm{m}} < 0$ for $r/L = 2$ and $F_{\mathrm{m}} > 0$ for $r/L = 1$), anisotropic attraction and repulsion (F_{m} varies between attraction and repulsion at different directions). **(c)** Typical examples from simulations show how the magnetic interactions differ between states. Red curve is where $F_{\mathrm{m}} = 0$, a closed red curve is indicative of cohesive interactions. Arrows indicate the direction of magnetic interaction forces at a given $\boldsymbol{r}$. Color bar indicates the strength of magnetic force, F_{m}/F_0. **(d)** Magnetic interaction force plots for the cohesive states used in the experiments. **(e, f)** Magnetic interaction states for n = 2 and n = 5 show that the range of Ψ for cohesive interactions change. **(g)** Steady-state distance, $F_{\mathrm{m}}(r^*) = 0$, changes with n.

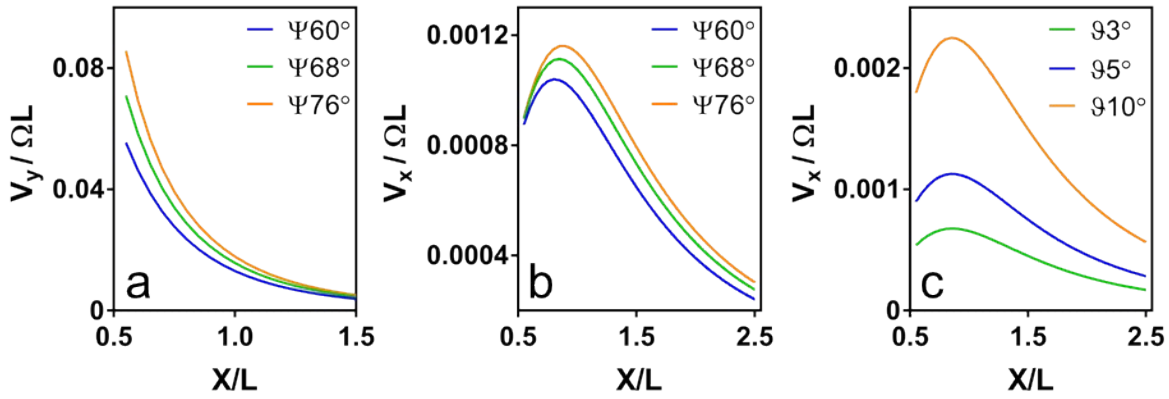

Figure S3. Flow velocity around a precessing chain near a surface. Simulated flow velocity is sampled along the line $x > 0, y = 0, z = 0.5L$ corresponding to the coordinate system shown in Figs. 2c-d. **(a)** Velocity of the rotational flow in y direction resulting from the chain precession about an axis perpendicular to the substrate for different precession angles Ψ. **(b, c)** Flow velocity in x direction when the chain precession axis is tilted by angle ϑ. **(b)** $\vartheta = 5^\circ$ for varying Ψ, **(c)** $\Psi = 70^\circ$ for varying ϑ.

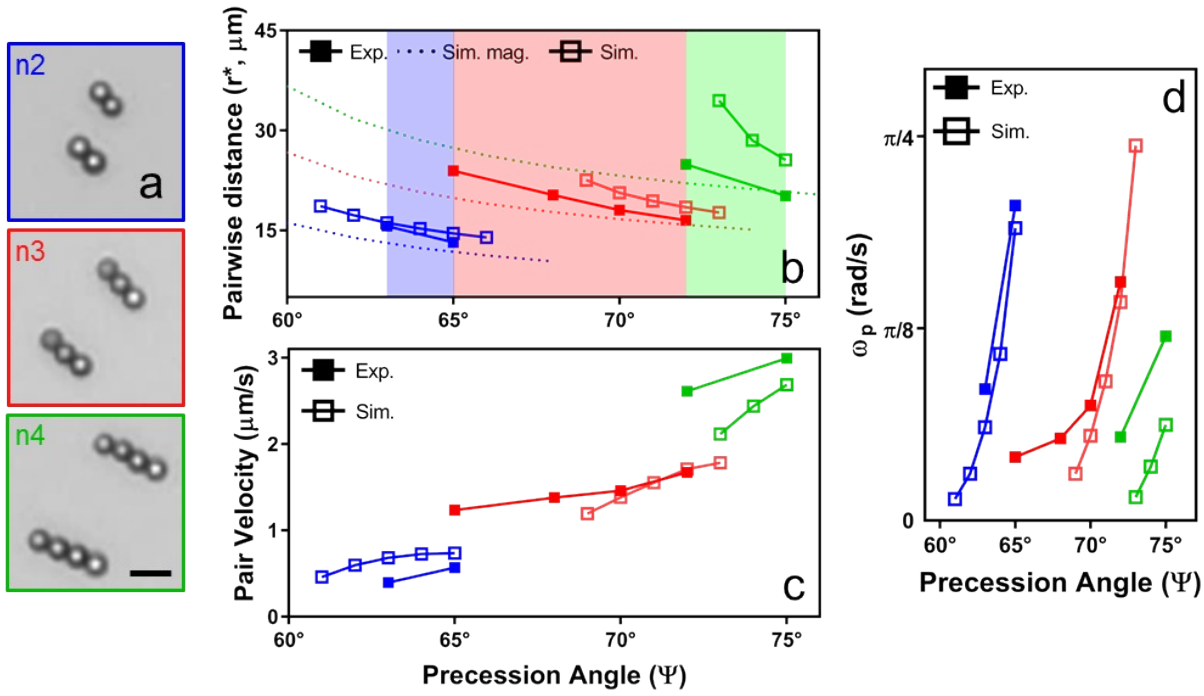

Figure S4. Experimental and simulated pairwise chain dynamics for different chain lengths. **(a)** Experimental snapshot of a pair of chains with different number of particles, *n*. Scale bar is 10 μm. **(b)** Pairwise steady-state distance, r^*, for different *n* and Ψ. Experimental measurements are compared to simulations including only magnetic interactions (Sim. mag.) and simulations that combined magnetic and hydrodynamic interactions (Sim.). Background color indicates the range of Ψ for experimentally observed cohesive self-organization state (*n* = 2, blue, *n* = 3, red, *n* = 4, green). **(c)** Pair translation velocity and **(d)** pair angular velocity measured from experiments and calculated with simulations. $\vartheta = 5^\circ$ for all figures.

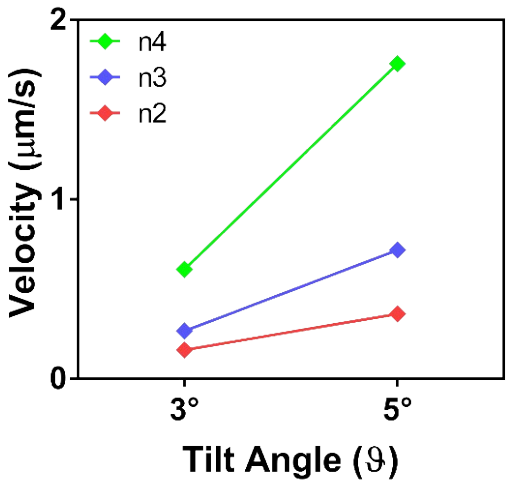

Figure S5. Experimentally measured single-chain velocities for different number of beads (*n*) and tilt angles (ϑ) at Ψ = 68°. Markers indicate the means obtained over time-series measurements.

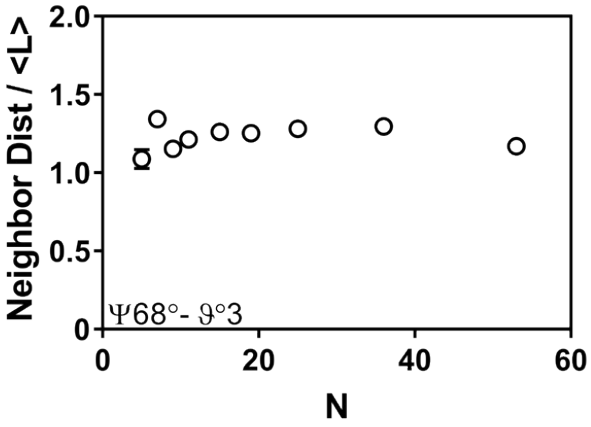

Figure S6. Mean neighbor distance does not vary significantly with cluster size (*N*). Nearest neighbors of each chain are detected via Delaunay triangulation. Error bars represent standard deviation of neighbor distances. Distances are normalized to the average chain length, < *L* >.

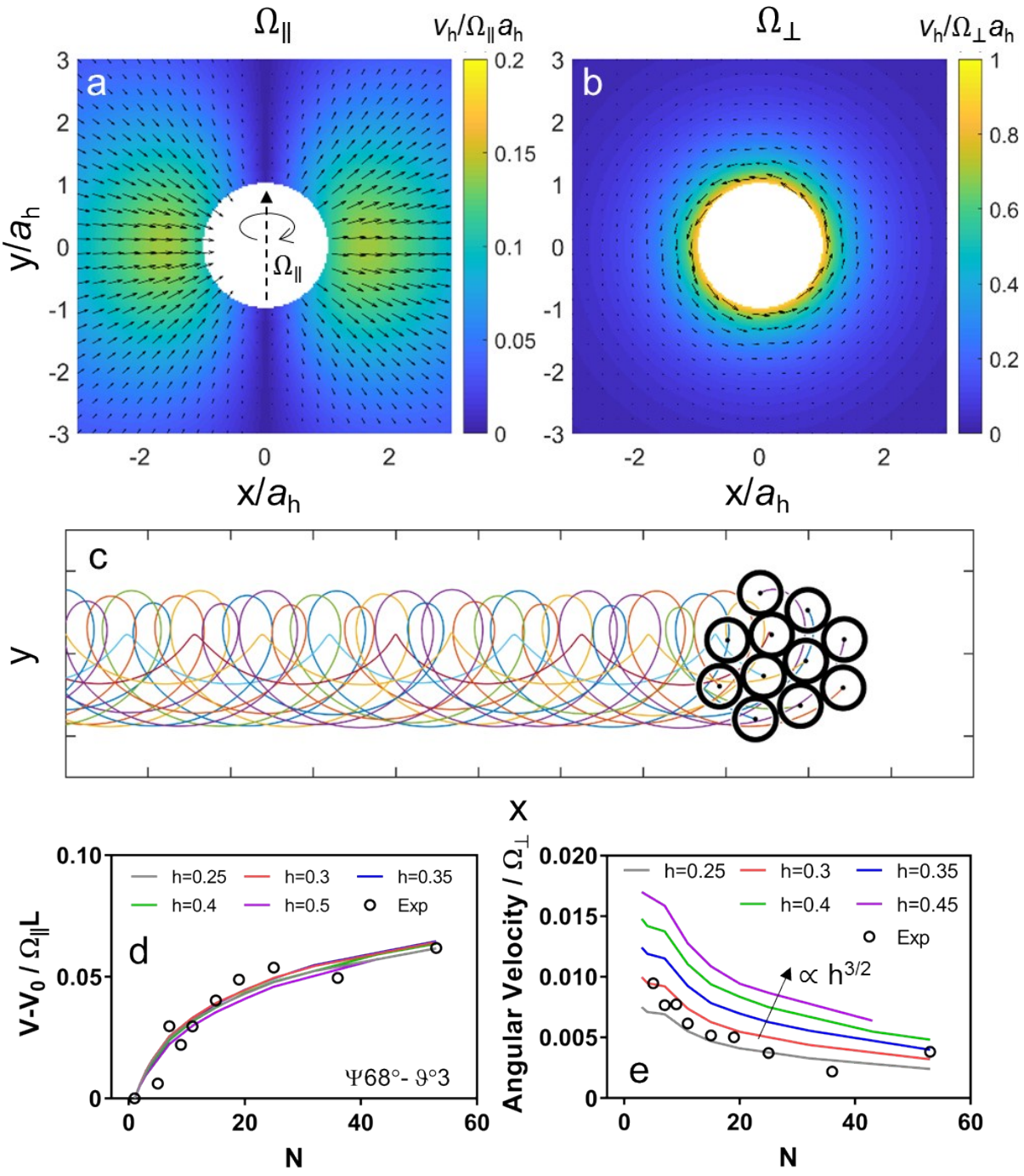

Figure S7. Reduced-order discrete chain model for simulating the cluster dynamics. Hydrodynamic field generated by each chain is modeled with a rotlet singularity above a planar no-slip wall. **(a)** Flow generated by a rotlet whose axis of rotation is aligned parallel to the substrate ($\Omega_{\parallel}$) and **(b)** perpendicular to the substrate ($\Omega_{\perp}$). Colorbar indicates normalized flow velocity

where a_h is the effective hydrodynamic radius of the chain. **(c)** A typical set of chain trajectories under cohesive interactions, as produced by the reduced order model. The diameter of each circle is equal to r^*, the steady-state distance term in Eq. S17. Reduced-order model captures experimentally observed changes in **(d)** cluster translation velocity (V) and **(e)** angular velocity with increasing cluster size N. v_0 is the velocity of an individual chain. Model is tuned for different heights of chains from the substrate surface, h.

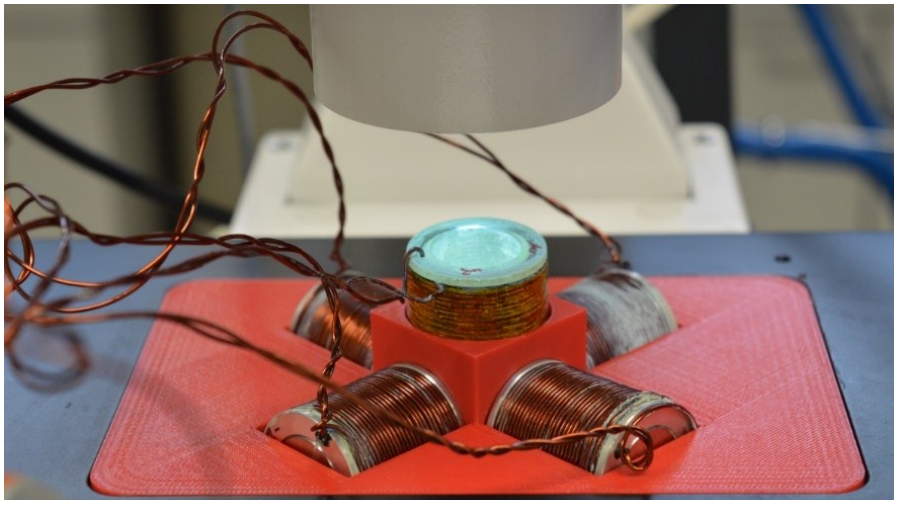

Figure S8. Photo of the experimental setup composed of five electromagnetic coils mounted on an inverted optical microscope.

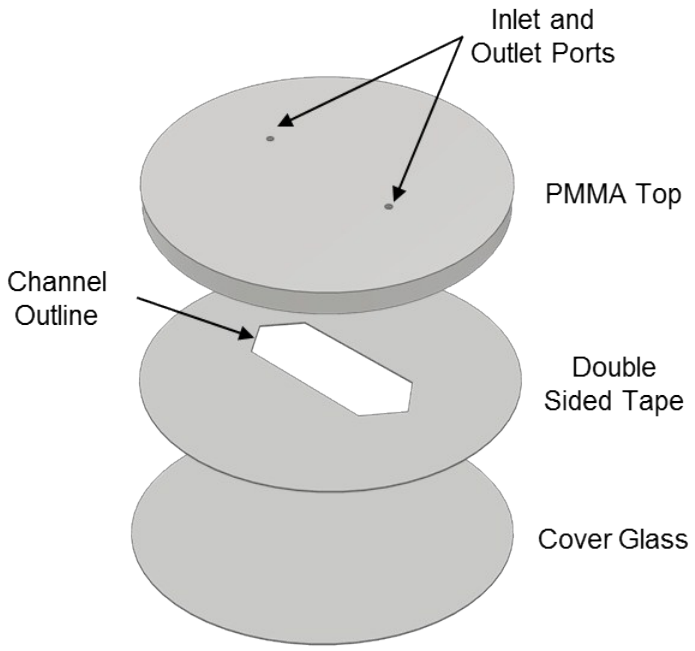

Figure S9. Schematic of microchannel design used in experiments. Inlet and outlet ports in PMMA top piece and channel outline in double sided adhesive tape were laser micromachined. All parts were then assembled, forming the microchannel.

Supplementary Videos

Video S1. Self-organizing cohesive microrobot collectives with multipolar interactions. Ψ denotes precession angle and ϑ denotes tilt angle of the time-varying magnetic field.

Video S2. Reversible assembly, clustering, de-clustering, and disassembly of chain microrobots and clusters.

Video S3. Simulated pair dynamics. Motion of two chains interacting magnetically and hydrodynamically above a solid substrate (at $z = 0$).

Video S4. Motion of homogeneous clusters. Clusters formed by a varying number of chains (N) are actuated at two different precession angles Ψ. Chain distances decrease with Ψ, and clusters translate faster with increasing N and Ψ.

Video S5. Motion and internal dynamics of heterogeneous clusters. A planar solid surface is located at z=0. Clusters with a higher level of heterogeneity (Het2) dissolve when actuated with $\vartheta = 5^{\circ}$, but remain intact when translation velocity decreased at $\vartheta = 3^{\circ}$. Experimentally measured internal chain positions are displayed with (bottom row) and without (top row) subtracting cluster rotation. Colors indicate number of particles in the corresponding chain, red: 2 particles, blue: 3 particles, green: 4 particles. Spatiotemporal organization of chains indicate a solid-like ordering for stable clusters.

Video S6. Formation of large groups.

Video S7. Cluster velocity increases with group size (N). Experimentally measured internal chain positions are displayed with (bottom row) and without (top row) subtracting cluster rotation. Colors indicate number of particles in the corresponding chain, red: 2 particles, blue: 3 particles, green: 4 particles, magenta: 5 particles. Large positional fluctuations of chains indicate a transition towards liquid-like behavior for larger clusters.

Video S8. Simulated cluster dynamics with the reduced-order model.